That is, for nonforward angles the Froissart bounds, and even the improved bounds of Kinoshita *et al.*, prove to be excessively weak. For our production differential cross section $d\sigma/d\Omega$, however, the experimental situation is less clear. But if Regge behavior is relevant for production processes, it may be that $d\sigma/d\Omega$ at nonforward angles falls only polynomially with s, rather than exponentially. Consider for example a production reaction with three particles in the final state: $p_1+p_2\to k+k_1+k_2$. Let k be the four-momentum of the distinguished particle; and define the subenergies $s_1=(k+k_1)^2$, $s_2=(k+k_2)^2$, as well as the momentum transfers $t_1=(p_1-k_1)^2$, $t_2=(p_2-k_2)^2$. It has been conjectured that the production amplitude displays Regge-like behavior, in the form $\text{Amp}\sim s_1^{\alpha(t_1)}s_2^{\alpha(t_2)}$, for the limit $s\to\infty$, with t_1, t_2 held finite. Now it is kinematically possible, even when the production angle θ of the distinguished particle is nonforward, for t_1, t_2 to be finite as $s\to\infty$, with $s_1\sim s$, $s_2\sim s$. Since $d\sigma/d\Omega$ involves an integration over all final-state variables other than θ, the differential cross section receives contributions from this Regge-like region of phase space. The corresponding s dependence of $d\sigma/d\Omega$ would then be polynomial rather than exponentially falling.

PHYSICAL REVIEW VOLUME 167, NUMBER 5 25 MARCH 1968

Use of Analyticity in the Calculation of Nonrelativistic Scattering Amplitudes*†

L. SCHLESSINGER‡
Department of Physics, University of California, Berkeley, California
(Received 25 October 1967)

A new method of calculating nonrelativistic scattering amplitudes is presented. The scattering amplitude is first calculated as a function of the complex energy below the scattering threshold, and the numerical results are then analytically continued to the physical region. The method is used to calculate two-body and two-channel scattering amplitudes. The numerical analytic continuation is accomplished by a rational-fraction representation similar to the Padé method. Several techniques of numerical analytic continuation by rational fractions are described, and some examples are discussed.

I. INTRODUCTION

THE analytic properties of the solutions of the Schrödinger equation have been extensively studied, but they have rarely been used in an actual calculation. In an earlier communication,[1] we described the preliminary results of a method which uses the analytic properties of the nonrelativistic scattering amplitude $T(W)$ as a function of the complex-energy variable W to calculate physical scattering amplitudes. In this paper, we give a more complete discussion of the method, and we apply it to the calculation of one- and two-channel scattering problems.

The method consists of two steps. First, $T(W)$ is found for a number of unphysical ($W<0$) values of W for fixed and physical values of the external momenta. Then these numerical results are analytically continued, using a rational-fraction approximation, to the physical energy region to obtain scattering phase shifts and amplitudes. Because the amplitude is calculated in the unphysical energy region where momentum-space integral equations of the Lippmann-Schwinger[2] type are nonsingular or coordinate-space variation principles of the Kohn[3] type have no complicated scattered-wave terms, the first step in the calculation is considerably easier than the direct solution of the Schrödinger equation. The rational-fraction approximation, which constitutes the second step of the method, is a simple and accurate technique for accomplishing the analytic continuation. This approximation is an important part of our method, and because it has a number of advantages over the standard methods of numerical analytic continuation, we discuss the methods we have devised to represent a function by a rational fraction in some detail.

The method of calculating scattering amplitudes is straightforward to use and yields accurate results. Moreover, it can be applied with only minor modifications to two-body, two-channel, and three-body scattering. Although the two-body problem has been discussed and solved many times,[4–6] and the results obtained here are not new, the discussion of this method in the

* Supported in part by the National Aeronautics and Space Adminstration and AFOSR, Office of Aerospace Research Grant No. AF-AFOSR-130-66.

† Work based on a thesis submitted by the author to the faculty of the University of California, Berkeley, in partial fulfillment of the requirements for the degree of Doctor of Philosophy.

‡ Present address: Department of Physics, University of Illinois, Urbana, Ill.

[1] L. Schlessinger and C. Schwartz, Phys. Rev. Letters **16**, 1173 (1966).

[2] B. A. Lippmann and J. Schwinger, Phys. Rev. **79**, 469 (1950).

[3] See T.-Y. Wu and T. Ohmura, *Quantum Theory of Scattering* (Prentice-Hall, Inc., Englewood Cliffs, N. J., 1962), Sec. D.

[4] C. Schwartz, Ann. Phys. (N. Y.) **16**, 36 (1961).

[5] R. Sugar and R. Blankenbecler, Phys. Rev. **136**, B472 (1964).

[6] H. P. Noyes, Phys. Rev. Letters **15**, 538 (1965).

simplest case clearly demonstrates both the advantages and limitations of this technique. The three-body calculations we have done—electron hydrogen scattering and the scattering of three particles interacting through Yukawa potentials—will be presented in a subsequent communication.

The paper is divided into several sections. Section II is a presentation of some methods used to effect the numerical analytic continuation by rational fractions. Three methods employed to accomplish this continuation are described and some simple examples are given. In Sec. III, we present the application of these methods to the solution of the two-body Schrödinger equation. Phase shifts for s-wave scattering in a Yukawa potential are calculated and are compared to those obtained by other methods. Section IV is a discussion of this method as applied to a two-channel nonrelativistic scattering problem with Yukawa potentials. Section V is a brief summary and conclusion.

II. NUMERICAL ANALYTIC CONTINUATION USING RATIONAL FRACTIONS

Numerical analytic continuation is an important step in our approach to the calculation of scattering amplitudes. This section is a discussion of a number of methods of numerical analytic continuation using rational fractions and a presentation of some numerical examples of this technique.

The problem considered here is the numerical analytic continuation of a function $f(x)$, given the values of the function at the K points x_i $(i=1\cdots K)$. Although the standard polynomial methods of continuation[7] are useful in proving that a unique continuation exists, they are not of great value in practice because small errors in the initial values of the function produce large errors in the continued values. Continuation using rational fractions has several advantages over these standard techniques. The asymptotic form of a rational fraction is bounded by some small power of x, and any knowledge of the large-distance behavior of $f(x)$ may be directly incorporated into this representation. The global bound imposed on the approximating function by the rational-fraction form inhibits the growth of the continuation error characteristic of polynomial expansions. Furthermore, a rational-fraction approximation can exactly reproduce polar singularities, thus extending the "radius of convergence" of the representation to the first nonpolar singularity of $f(x)$. Even the nonpolar singularities of the function may be well approximated by poles and zeros of the rational fraction, affording a good representation of the function far from these singularities.

One well-known technique of numerical analytic continuation by rational fractions, which has been used successfully in the solution of a number of physical problems, is the Padé approximant method. (For a good discussion, see Baker.[8]) The use of this method, however, requires the coefficients of the Taylor's-series expansion of $f(x)$. The three methods we have devised for the representation of $f(x)$ by rational fractions are similar in spirit to the Padé method but use only the values of the function at a set of points and not its Taylor's-series representation. We have called these techniques the norm method, the moment method, and the point method, and they are described in the following paragraphs.

Let $R_{N,M}(x)=P_N(x)/Q_M(x)$ be the N,M rational approximation to $f(x)$. $P_N(x)$ is the Nth-order polynomial in x which forms the numerator of the fraction, and $Q_M(x)$ is the Mth-order polynomial in x which forms the denominator of the fraction. The norm method determines $R_{N,M}(x)$ so that the norm of the function $f(x)Q_M(x)$-$P_N(x)$ is a minimum under variation of P_N and Q_M. For this method, we let

$$P_N(x)=\sum_{k=0}^{N} p_k u_k(x),$$

$$Q_M(x)=1+\sum_{k=1}^{M} q_k u_k(x),$$

where $u_i(x)$ are orthogonal polynomials with the weight function $w(x)$ over the interval (a,b), which includes x_i $(i=1\cdots K)$. That is,

$$\int_a^b u_n(x)u_m(x)w(x)dx=\delta_{nm}.$$

The condition we impose is that

$$I(q,p)=\|f(x)Q_M(x)-P_N(x)\| = \int_a^b w(x)\,|f(x)Q_M(x)-P_N(x)|^2 dx \quad (2.1)$$

is a minimum under variation of the q's and p's. Doing the variation, we obtain

$$\frac{\delta I}{\delta q_j}=\int_a^b w(x)f(x)[f(x)Q_M(x)-P_N(x)]u_j(x)dx=0,$$

$$\frac{\delta I}{\delta p_j}=\int_a^b w(x)[f(x)Q_M(x)-P_N(x)]u_j(x)dx=0.$$

Defining

$$\int_a^b w(x)u_n(x)u_m(x)f(x)\equiv f_{nm},$$

[7] R. V. Churchill, *Introduction to Complex Variables and Applications* (McGraw-Hill Book Co., Inc., New York, 1948).

[8] W. Baker, in *Advances in Theoretical Physics, V*, edited by K. Brueckner (Academic Press Inc., New York, 1965), Vol. I, pp. 1–58.

and noting $q_0=1$, we have

$$\sum_{k=0}^{M}(f^2)_{jk}q_k-\sum_{k=0}^{N}f_{jk}p_k=0, \tag{2.2}$$

$$\sum_{k=0}^{M}f_{jk}q_k-p_j=0. \tag{2.3}$$

Substituting (2.3) into (2.2) yields

$$\sum_{k=0}^{M}(f_{jk}{}^2-\sum_{l=0}^{N}f_{jl}f_{lk})q_k=0, \quad j=1\cdots M. \tag{2.4}$$

Since $q_0=1$, Eq. (2.4) is a set of M linear equations for the M unknowns $q_1\cdots q_M$. Substituting these q's into (2.3) determines the p's. The condition (2.1) is thus sufficient to determine a rational-fraction approximation to $f(x)$.

The input to this method is the values of $f(x)$ at the K points $x_1\cdots x_K$. These points are chosen to facilitate accurate numerical evaluation of the integrals for the matrix elements f_{nm}. One method of obtaining these integrals is numerical quadrature (based on the polynomials u_i), which requires the x_i to be the K roots of the polynomial $u_K(x)$. The moment method also uses these numerical integration techniques.

The moment method determines the coefficients of the rational-fraction approximation to $f(x)$ by requiring the first $N+M+1$ moments of the expression $f(x)Q_M(x)-P_N(x)$ to be zero. Using the same notation as for the norm method, this may be written as

$$\sum_{k=0}^{N}p_ku_k(x)=f(x)\sum_{k=0}^{M}q_ku_k(x), \tag{2.5}$$

where q_0 and u_0 equal 1. Multiplying (2.5) by $u_j(x)w(x)$ and integrating, we obtain

$$p_j=\sum_{k=0}^{M}f_{jk}q_k, \quad j=0\cdots N \tag{2.6}$$

and

$$\sum_{k=1}^{M}f_{jk}q_k=-f_{j0}, \quad j=N+1\cdots N+M. \tag{2.7}$$

Equation (2.7) is a set of M linear equations for the M unknown q's. Using the solutions of (2.7) in (2.6) determines the p's. If the polynomials $u_i(x)$ are chosen to be $1, x, x^2, \cdots$ over the unit circle, then this method (with the appropriate modifications for complex polynomials) is the same as the Padé approximant method for a function which has a convergent power series in the unit circle.

In the preceding methods, we actually make two approximations. First, the integrals of $f(x)$ are represented as finite sums; then $f(x)$ is represented as a rational fraction, using these approximate integrals. In practice, the norm method suffers most from this double approximation because of the many manipulations of the matrix elements f_{nm}; the moment method works quite well despite this limitation. It is desirable, however, to have a method which is more straightforward than the preceding ones.

The point method is a direct approach to the representation, we simply set

$$f(x_i)=P_N(x_i)/Q_M(x_i), \quad i=1\cdots N+M+1 \tag{2.8}$$

where

$$P_N(x)=\sum_{k=0}^{N}p_kx^k,$$

$$Q_M(x)=1+\sum_{k=1}^{M}q_kx^k.$$

Rearranging (2.8), we obtain a set of $N+M+1$ linear equations for the $N+M+1$ unknown p's and q's. In this case, $R_{N,M}(x)$ is determined so that $R_{N,M}(x_i)=f(x_i)$ at the $N+M+1$ points x_i.

A more efficient means to effect the point type of representation is obtained using continued fractions. As before, we have K values of $f(x)$, and we want to represent $f(x)$ as $R_{N,M}(x)$, so that $R_{N,M}(x_i)=f(x_i)$ at the K points $x_1\cdots x_K$. To do this, consider the continued fraction

$$C_N(x)=\frac{f(x_1)}{1+}\,\frac{a_1(x-x_1)}{1+}\,\frac{a_2(x-x_2)}{1+}\cdots\frac{a_N(x-x_N)}{1}. \tag{2.9}$$

It is easy to see that $C_N(x_1)=f(x_1)$ and that the coefficients $a_1\cdots a_N$ can be chosen so that $C_N(x_i)=f(x_i)$. We show in the Appendix that the coefficients a_l in (2.9) may be determined recursively from the formula

$$a_l=\frac{1}{(x_l-x_{l+1})}\left\{1+\frac{a_{l-1}(x_{l+1}-x_{l-1})}{1+}\,\frac{a_{l-2}(x_{l+1}-x_{l-2})}{1+}\cdots+\frac{a_1(x_{l+1}-x_1)}{1-[f(x_1)/f(x_{l+1})]}\right\} \tag{2.10}$$

and

$$a_1=\{[f(x_1)/f(x_2)]-1\}/(x_2-x_1).$$

Equations (2.9) and (2.10) form a simple, fast, and efficient algorithm for representing $f(x)$ as a rational fraction.

The rational-fraction representations described above are generally used to form a sequence of approximations to the desired function as the order of the polynomials in the numerator and denominator are increased, keeping $N-M$ fixed. The norm and moment methods have the advantage that they use all the input points $x_1\cdots x_K$ at each stage of the approximation. The disadvantages of these methods are that the double approximation involved leads to large numerical round-off errors, especially for the norm method, and that the location of the input points is fixed by the numerical

integration techniques. The point methods are more straightforward to use; they do not involve a double approximation, and they are more flexible because the input points are arbitrary and can be chosen to best represent the function.

Comparison of Methods and Examples

There is no general theory which describes either the convergence or the convergence rates of the type of rational approximations described here. In the following paragraphs, we discuss some simple examples to establish a number of rules for the use of these methods.

We expect this type of representation to be able to approximate a rational fraction exactly, but, because a rational fraction can have only one sheet in the complex plane, we could not hope to approximate a many-sheeted function everywhere. Our approximation can, however, yield a good representation of a function on a single sheet. In general, a branch line is approximated by a succession of poles and zeros of a rational fraction, and far from the branch line, the approximation is quite good. For the functions studied, the region of convergence of this representation appears to be everywhere on one sheet of the complex plane, except for a small region surrounding the branch line.

The examples given here were computed by taking values of simple functions at several points along the positive axis from $z=0$ to $z=\infty$, applying the methods previously discussed, and evaluating the resulting rational fraction along the negative z axis as shown in Fig. 1. To obtain a fair comparison, the same points and the same numerical accuracy were used for all the methods. We included the bound on our rational fractions by requiring whenever possible that the rational fraction and the function go as the same power of z at large z. The first example, Fig. 2, is a graph of the fractional error $f(z)-R_{5,5}(z)/f(z)$ versus the distance from $z=-1$ for the rational approximation to $f(z)=[z/(1+z)]^{1/2}$. In this case, we can match the power behavior of $f(z)$ because both $f(z)$ and $R_{5,5}(z)\to$ constant. In this, as in all the examples tried, the norm method suffered from numerical roundoff errors and gave results consistently worse than the other methods. For this reason it is not useful for numerical computations, and to avoid confusion, it is left out of most subsequent graphs and discussions. Figure 3 shows a graph of several high-order, high-accuracy (12-place arithmetic) continued-function approximations to $[(z+1)(z-2)]^{-1/2}$. By including the correct asymptotic form of the function into the rational approximation, the propagation of errors characteristic of the polynomial analytic continuation is eliminated. To demonstrate the importance of having the correct asymptotic behavior, we show in Fig. 4 the [5,5] and the [5,4] continued-fraction approximations to

$$\{[(1+z+z^2)(1+2z)]^{1/3}-1\}/z.$$

In this example, we have plotted the fractional error versus the distance from $z=0$. The rational approximation with the correct asymptotic behavior gives a good representation of the function everywhere on one sheet of the complex plane except very near the cut at Real $z=-0.5$, while the approximation with the wrong asymptotic form exhibits the polynomial-like behavior discussed before.

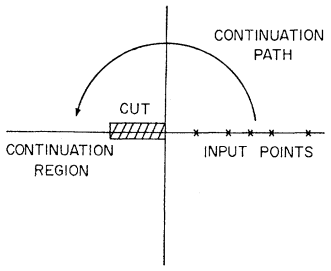

FIG. 1. Location of input points, branch out, continuation path, and output region for some of the examples described in Sec. II.

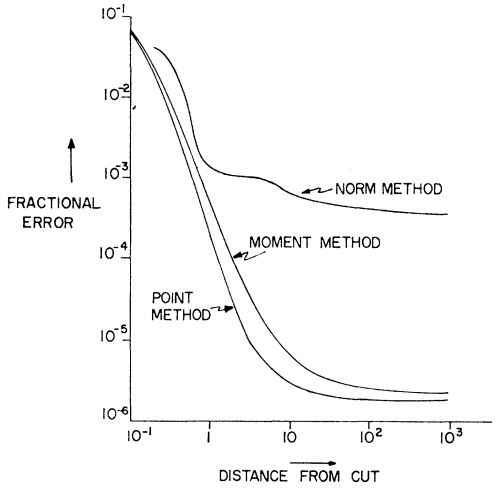

FIG. 2. Fractional error versus distance from $z=-1$ for norm, moment, and point method of approximation to $[z/(1+z)]^{1/2}$. The order of approximation $N=5$.

In general, the representation converges rapidly as a function of the order of approximation N for both the moment and point methods, and the error, as a function of N, is approximately independent of the distance from the branch point. Note that even though the gross nature of the error as a function of N is rapidly decreasing, the convergence is not always monotonic, and there are isolated values of N for which both the $N-1$ and $N+1$ approximants have a smaller error. This behavior seems to be a general feature of any rational approximation and is also encountered in the Padé method. As pointed out in Ref. 8, the $[3N+1, 3N+1]$ Padé approximants to $[(1+x+x^2)(1+2x)]^{1/3}-1/x$ do not exist. For our methods, the representation

exists except for special cases, but may be quite poor for particular values of N. In practice, if a member of a sequence is noticeably out of line with its neighbors, it may be interpreted as one of these singular values of N and may be safely ignored.

In all the examples we tried, the moment and point methods yielded comparable errors and rates of convergence. However, the continued-fraction method is faster and easier to use than the moment method. Furthermore, it has an extra degree of freedom because one is at liberty to choose the location of the input points. The use of this degree of freedom can result in more accurate continuations. For these reasons, the continued-fraction method is considered the most useful of all the methods proposed, and it is the method we used in our calculation of scattering amplitudes.

From the previous examples it is clear that the accuracy of the continuation is greatest at large

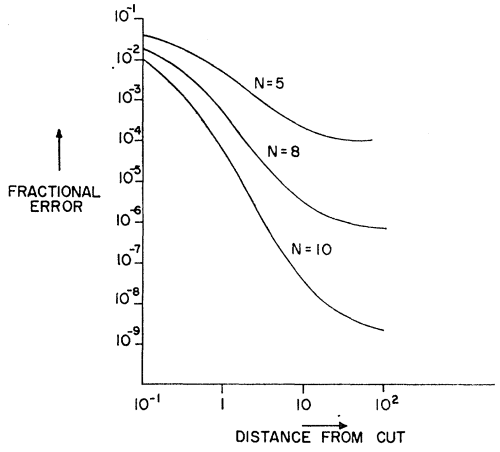

FIG. 3. Fractional error versus distance from $z=-1$ for high-order, high-accuracy continued-fractions approximation to $[(1+z)(2-z)]^{-1/2}$. The orders of approximation $N=5$, 8, 10.

distances from the singularities of the function. In the preceding examples, the input points were distributed "evenly"[9] over the positive z axis as required by the moment method. This last result, however, suggests that to obtain the most accurate approximation to a function at a particular point a, one should distribute the input points evenly over the transformed input region in the plane where the point $z=a$ is infinitely far from the singularities of the function. As an example, we use the function $\ln\{(1+z^2)/(4+z^2)\}$. To get an accurate approximation to this function at $z=a$, we use the transformation $y=z/(z-a)$. In the y plane, the singularities are infinitely far from the point in question, and the input points ($z=0$ to $z=\infty$) are mapped into the line $y=0$ to $y=1$ for $a<0$. The results using the input points obtained in this way for the values $a=-0.5$ and

[9] The polynomials used for the norm and moment methods were Laguerre polynomials. The evenly distributed points were obtained as the zeros of the 15th Laguerre polynomial.

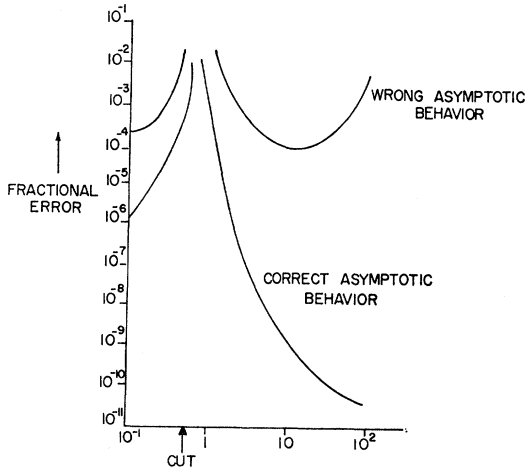

FIG. 4. Fractional error versus distance from $z=0$ for point method of approximation to $\{[(1+z+z^2)(1+2z)]^{1/3}-1\}/z$. The cut is located at $\mathrm{Re}z=-0.5$.

$a=-10$ are shown in Fig. 5, along with the results for the evenly distributed points. From these graphs we see that picking the input points in this way gives an improved approximation in the neighborhood of the point mapped to infinity, but only at the expense of the points elsewhere in the complex plane.

Finally, we consider the approximation of an essential singularity. The first example studied was the function e^{-z}. As before, this function was approximated by taking a number of points along the positive axis as input and evaluating the resulting rational fraction along the negative z axis. For this function the method failed. This failure, we believe, is obtained because the function has very different large-z behavior along the input direction and the continuation direction in the z plane. The Padé method or the moment method using the polynomials 1, x, x^2, $\cdots$ over the unit circle should be able to approximate e^{-z} well over a limited region, since they use values of the function taken only in a small

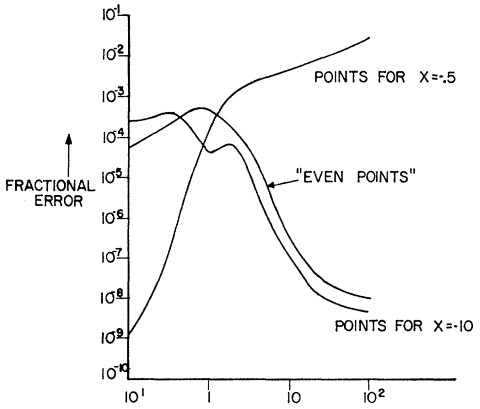

FIG. 5. Fractional error versus distance from $x=0$ for point method of approximation to $\ln[(1+x^2)/(4+x^2)]$ for input points picked in several ways. The order of approximation $N=5$.

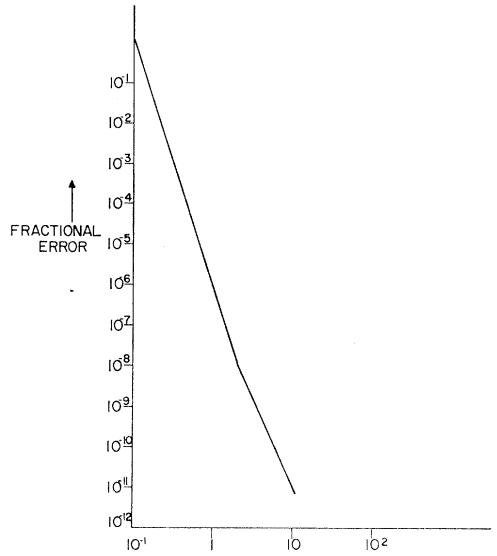

FIG. 6. Fractional error versus distance from $z=0$ for point method of approximation to $e^{z/(1+z)}$. $N=4$.

region in the complex plane. According to the above remarks, our methods should be able to approximate a function like $e^{z/1+z}$ quite well. Figure 6, the graph of the fractional error versus z for this function, supports this claim. The rational approximation converges rapidly outside a small region surrounding the essential singularity.

From these examples we can see that the rational-fraction technique is a powerful approach to numerical analytic continuation. The rational-fraction approximations that we have tried can represent most functions quite well on one sheet of the complex plane. The moment and point methods yield comparable results, while the norm method is less useful because of numerical roundoff errors. The point methods are generally the easiest to use and the most flexible.

III. TWO-BODY SCATTERING

In this section, we use the methods of numerical analytic continuation to calculate two-body–nonrelativistic-scattering phase shifts. We first present a discussion of the method and some of the techniques used in its application. Finally, we present the results of the calculations and compare them to the results obtained by other methods.

A. Continuation Method

The continuation method makes use of the analytic properties of the T matrix as a function of the complex-energy variable W to determine scattering phase shifts. To begin, we consider the Schrödinger equation in the form

$$(E-H)\Psi_p=0, \tag{3.1}$$

with the decomposition

$$H=H_0+V \tag{3.2}$$

and the plane-wave states φ_p, labeled by the physical momentum of the scattered particle, which satisfy

$$(E-H_0)\varphi_p=0. \tag{3.3}$$

Here $E=p^2/2m$ is the physical energy of the particle of mass m and momentum p. The T matrix or scattering amplitude is defined as a function of the complex-energy variable W as

$$T(W)=V+V(W-H_0)^{-1}T(W). \tag{3.4}$$

The physical-scattering amplitude for the transition $p\longrightarrow p'$ is obtained as the limit of the matrix elements of the T operator between the plane-wave states φ_p and $\varphi_{p'}$ as W approaches the physical energy from above in the complex plane. That is,

$$T(p',p,E)=\lim_{W\to E+i\epsilon}(\varphi_{p'},T(W)\varphi_p). \tag{3.5}$$

The formal solution to (3.4) may be written as

$$T(W)=V+V(W-H)^{-1}V. \tag{3.6}$$

Knowing the spectrum of the operator H, we can conclude that $T(W)$ may have simple poles, corresponding to the bound states of H, for real negative values of W, and it has a line of discontinuities, corresponding to the scattering states of H, along the positive real W axis. Everywhere else on the first sheet of the W plane $T(W)$ is analytic.

The method consists of two steps: (1) Calculate $T(W)$ at several real negative values of W; (2) analytically continue these numerical results to $W=p^2/2m+i\epsilon$ to obtain physical-scattering phase shifts (as shown in Fig. 7).

The calculations involved in the first step are much easier to perform than in the ordinary methods. From Eq. (3.4) we see that for $W<0$ the integral equation for $T(W)$ is nonsingular and may be solved by straightforward mesh-point integration. In the coordinate representation, we must solve the inhomogeneous

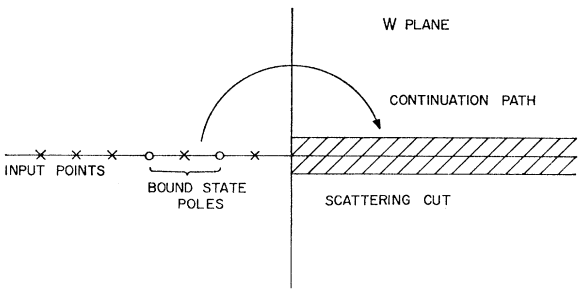

FIG. 7. Analytic structure of the two-body scattering amplitude in the complex-energy plane.

Schrödinger equation

$$(W-H)\Psi_p(W)=(W-H_0)\varphi_p. \tag{3.7}$$

Writing $\Psi_p(W)=\chi_p(W)+\varphi_p$, Eq. (3.7) becomes

$$(W-H)\chi_p(W)=V\varphi_p, \tag{3.8}$$

from which we may obtain $T(W)$ as

$$T(p',p,W)=(\varphi_{p'},V\varphi_p)+(\varphi_{p'},V\chi_p(W)).$$

For $W<0$ the asymptotic form of $\chi_p(W)$ is that of a decaying exponential,[10] and the use of the complicated asymptotic term, necessary in the Kohn method, is avoided.

Any method of calculating scattering amplitudes must deal with the singularity of $T(W)$ at threshold ($W=0$ in this case). The effect of this singularity manifests itself in the Kohn method as a constraint on the asymptotic form of the coordinate-space trial wave functions. The mesh-point method of Noyes[6] uses a modification of the kernel of (3.4) to make it nonsingular near $W=0$, but involves the solution of an auxiliary equation. In our method, this singularity is taken into account in the second step of the calculation. By examination of the Born series for $T(W)$, one can show that $T(W)$ has a simple square-root branch point at $W=0$.[11] To continue $T(W)$ to $W>0$, we represent it as the ratio of polynomials in $\sqrt{(-W)}$, using the rational-fraction techniques discussed before. Representing $T(W)$ in this way not only accounts for the singularity at $W=0$, but also reproduces its polar singularities quite well. The nonpolar singularities of $T(W)$ are represented by poles and zeros of the rational fraction, and can give an accurate approximation for T far from these singularities.

B. Methods of Calculation

There are several ways to calculate the input to this method, the values of $T(W)$ at a number of points $W_i<0$. In the momentum representation, the partial-wave projection of (3.4) is

$$T_l(p,p,W)=V_l(p,p)+\int_0^\infty V_l(p,p')\frac{p'^2}{W-(p'^2/2m)}T_l(p',p,W)dp'.$$

Since for $W<0$ this is a nonsingular integral equation, it may be solved by straightforward mesh-point integration. In coordinate space we use a modification of the Kohn method to obtain the input. The expression

$$T_l(p,p,W)=(\varphi_p{}^l,V\varphi_p{}^l)+(\varphi_p{}^l,V\chi_p{}^l)+(\chi_p{}^l,V\varphi_p{}^l)-(\chi_p{}^l,[W-H]\chi_p{}^l) \tag{3.9}$$

is stationary under variation of $\chi_p{}^l(W)$ and is equal to $T_l(p,p,W)$ when $\chi_p{}^l(W)$ satisfies (3.8).

[10] This calculation is done off the energy shell; thus $p^2\neq 2mW$, and p is always taken to be real and equal to its physical value.

[11] A. J. Dragt and R. Karplus, Nuovo Cimento **26**, 168 (1962).

To show how we solved (3.9), we pick the specific example of S-wave scattering in the potential $V=\lambda e^{-r}/r$, where (3.8) becomes

$$\left[\frac{1}{r}\frac{d^2}{dr^2}r+W-V\right]\chi_p{}^l(r)=\frac{\lambda e^{-r}}{r}\frac{\sin(pr)}{pr}. \tag{3.10}$$

We first pick a complete set of trial functions $\chi_i(r)$ and represent the Nth approximation to $\chi_p(r)$ in that basis as

$$\chi_p{}^{(N)}=\sum_{i=1}^{N}D_i\chi_i. \tag{3.11}$$

A good choice for the χ_i is $\chi_i(r)=r^{i-1}e^{-\alpha r}$, $i=1\cdots N$, which displays the correct behavior both as $r\to 0$ and ∞. For very small or very large values of W, many trial functions must be used to approximate the $e^{-r\sqrt{(-W)}}/r$ behavior of χ; thus, if a rapidly convergent approximation is desired at all values of W, the function

$$\chi_0=(e^{-r\sqrt{(-W)}}-e^{-\alpha r})/r$$

should be included in the set (3.11). For most purposes (3.11) is adequate.

We then form a matrix representation of (3.9) in the basis (3.11). The actual variation of parameters leads to the set of linear equations

$$H_{ij}D_j=V_i, \tag{3.12}$$

where

$$H_{ij}=\int\chi_i{}^l(r)\left(\frac{1}{r}\frac{d^2}{dr^2}r+W-V\right)\chi_j{}^l(r)r^2dr,$$

$$V_i=\int\chi_i{}^l(r)\frac{\lambda e^{-r}}{r}\frac{\sin(pr)}{pr}r^2dr.$$

The solution of (3.12) provides the Nth-order approximation to $\chi(W)$ which, when substituted in (3.9), gives the Nth stationary approximation to $T_l(p,p,W)$. These values are then used as input to one of the analytic-continuation methods previously discussed to obtain scattering phase shifts.

To do the continuation, we unfold the cut W plane by the transformation $y=\sqrt{(-W)}$. In the y plane the input is along the real y axis, and we are continuing to $y=-ip$ as shown in Fig. 8, where p is the physical momentum $p^2/2m=E$. There are an infinite number of ways to choose the location of the input points; a good set of points was obtained by mapping the continuation point to infinity as discussed in the previous section. The transformation

$$x=iy/(a+iy) \tag{3.13}$$

(with $a<0$) maps the scattering region into the entire real x axis, excluding the diameter of the semicircle formed by the mapping of the real positive y axis as shown in Fig. 9. The point $y=+ia$ is mapped to $-\infty$ in the x plane. Taking $a=-p$, this continuation point is

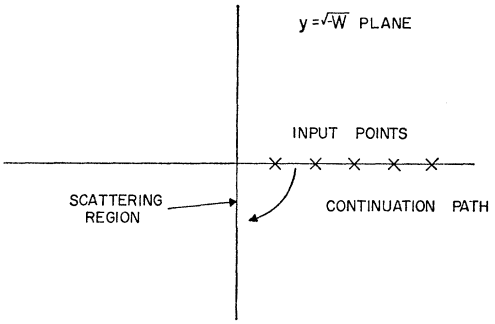

FIG. 8. Location of input points and continuation path in the $y=\sqrt{(-W)}$ plane.

mapped to $-\infty$ in the x plane. It should be clear that the points W_i used, for example, in the variational principle, still lie along the negative W axis. These transformations only choose a good distribution of the points for a particular momentum. In practice, one calculates the input for a number of values of the momentum simultaneously, and thus one set of input points is desirable. For this reason, we usually pick $a=-1$ in the transformation (3.13), although we do have some examples for $a=-p$.

An interesting feature of this approach for choosing the location of the input points occurs at $p=0$. Our prescription with $a=p=0$ forces all the input points to be at $W=0$. In fact, this is correct because for $p=0$, the T matrix element can be calculated directly as the limit as W approaches 0 from the negative direction; only one point, $W=0$, is necessary, and there is no need for continuation.

C. Results

The numerical examples chosen to describe this method for two-body scattering are the calculations of S-wave phase shifts with a Yukawa potential. The approximation to $(\tan\delta)/p$ was calculated, using the point or continued-fraction method for the sequence $N=1, 2, 3, \cdots$, where $2N+1$ is the number of input points at each stage. Since $T(W)$ approaches a constant

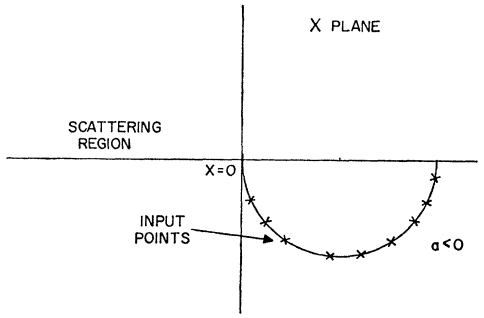

FIG. 9. Mapping of the $y=\sqrt{(-W)}$ plane under the transformation $x=iy/(a+iy)$, $a<0$.

TABLE I. Successive approximations to the scattering length $[-l=(\tan\delta)/p$ at $p=0]$ for the Yukawa potential $-2e^{-r}/r$. The scattering length given by the Kohn method is $-l$ (Kohn) $=-7.91138$.

	N (order of fitting)	$-l$ (even points)	$-l$ (transformed points)
Born approximation	0	+2	+2
	1	···	−7.8008537
	2	−7.95219	−7.9268039
	3	−7.90230	−7.9113300
	4	−7.91438	−7.9114034
	5	−7.91152	−7.9113759
	6	−7.91164	−7.9113797
	7	−7.91199	−7.9113816

(the Born term) as $W\to\infty$,[12] we used the rational fraction $R_{[N,N]}(\sqrt{-W})$ in its representation. In this case, N is also the order of the polynomials in the numerator and denominator of the rational fraction. The input points were obtained using the variational principle previously described, and their accuracy depends on the momentum of the particle.

In Table I, we compare the results of this type of calculation for λ, the potential strength, equal to -2 and p equal to 0. The entries in the first column of the table were calculated for the input points evenly distributed along the negative W axis; the entries in the second column were calculated using the input points given by the transformation (3.13), with $a=-1$. As discussed before, for $p=0$ the scattering length $[-l=(\tan\delta)/p$ as $p\to 0]$ may be calculated directly from the modified Kohn principle. The results of this calculation, a special case of (3.13), with $a=0$, yield $=+7.9113802$ to eight decimal places.

For p not equal to zero, the unitarity condition

$$\mathrm{Im}(T_l)^{-1}/p=1$$

is a very useful check on the calculation. In Tables II and III, we give the results of the calculation for the Yukawa potential of strength $\lambda=-2$ and for the momenta $p=0.5, 2$. The first three columns of each table show the calculated values of $(\tan\delta)/p$, using the point or continued-fraction method, and the last column shows the calculated value of

$$\mathrm{Im}(T_l)^{-1}/p,$$

which should be one. For column 1, the input points were distributed evenly along the negative W axis; for column 2, the input points were obtained according to the transformation (3.13), with $a=-1$; and for column 3, the input points were obtained from the transformation (3.13), with $a=-p$. Column 4 is the unitarity condition calculated using the last set of input points.

[12] It is not clear that the T matrix also goes to a constant as $W\to\infty$ on the second sheet. However, we pick the $[N,N]$ rational approximation to the T matrix to insure its correct asymptotic behavior on the first sheet in the W plane and to inhibit the growth of continuation errors. That this procedure gives a good approximation to the correct amplitude is verified using the unitarity condition discussed above.

TABLE II. Successive approximations to $(\tan\delta)/p$ and the unitarity condition for the Yukawa potential $-2e^{-r}/r$ for momentum $p=0.5$ for three distributions of the input points. The unitarity condition was calculated using only the last set of points. $(\tan\delta)/p$ (Kohn) = 16.8938.

N	$(\tan\delta)/p$ (even points)	$(\tan\delta)/p$ $(a=-1)$	$(\tan\delta)/p$ $(a=-p)$	Unitarity $(a=-p)$
1		10.875040	10.135518	0.97273549
2	13.2348	11.124486	11.132695	0.97840186
3	17.0897	16.938998	16.861517	1.0003043
4	16.8946	16.916398	16.894051	1.0000144
5	16.9067	16.893570	16.894088	0.99999968
6	16.8771	16.893569	16.893830	0.99999989
7	16.8571	16.893473	16.893834	1.00000000

The input points were accurate from 8–10 places for $p=0.5$ and 5–7 places for $p=2$. From the tables it is clear that the results are excellent for low momentum, but they are less precise as the momentum is increased. This is an example of the effect of the input accuracy. Comparison of the arithmetic precision of the input points and the results leads to the conclusion that an accuracy of about two decimal places is lost in the continuation.

These calculations for $\lambda=-2$ represent a good test of the method, since, at this value of the potential strength, there is a bound state of the system very close to $W=0$. We obtained the same good results for values of λ from -5 to $+5$ and p from 0 to 2.5. As an estimate of the computer time necessary for this type of calculation, we remark that the results of the type used above were calculated for $\lambda=-3, -2, -1, 1, 2, 3$ and $p=0$, 0.5, 1.0, 1.5, 2, 2.5 in 15 sec of CDC-6400 computer time.

In our discussion of the rational-fraction method, we claimed that this representation could fit a polar singularity quite well. To support this assertion, we tried to find the position of the first bound-state pole of the T matrix from the zeros of the denominator of the rational fraction. For the $[N,N]$ approximation there are N zeros in the denominator, but the zeros corresponding to the actual poles of the T matrix should remain stationary as the order of approximation is increased, while the other poles move in the complex plane. Since our representation is in the variable $\sqrt{(-W)}$, we are able to find not only the positions of

TABLE III. Successive approximations to $(\tan\delta)/p$ and the unitarity condition for the Yukawa potential $-2e^{-r}/r$ for $p=2$ and three distributions of input points. Unitarity was calculated using only the last set of points. $(\tan\delta)/p$ (Kohn) = 0.50.

N	$(\tan\delta)/p$ (even)	$(\tan\delta)/p$ $(a=1)$	$(\tan\delta)/p$ $(a=p)$	Unitarity $(a=p)$
1		0.5368	0.4534	0.3176
2	0.4543	0.5254	0.4876	0.7440
3	0.4861	0.5390	0.4982	0.9281
4	0.4868	0.4991	0.4936	0.9949
5	0.4946	0.4984	0.5001	0.9965
6	0.4985	0.5010	0.4957	1.0005
7	0.4986	0.5045	0.5015	1.0013

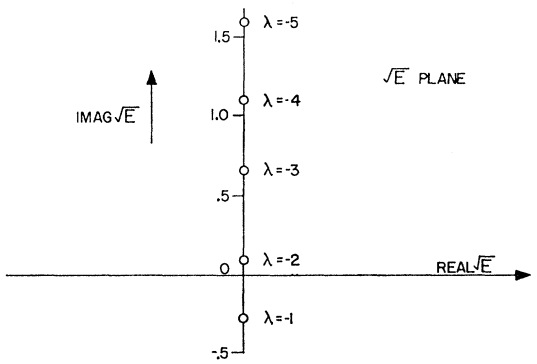

FIG. 10. Position of the first bound-state pole in $\sqrt{E}$ plane for various potential strengths λ as determined by the pole of the rational approximation.

the true bound states at $W<0$ on the first sheet of the W plane, but also the positions of some of the poles on the second sheet of the W plane. These poles correspond to states that will become bound as the potential strength is increased. For the S wave, as the attractive potential strength is increased from $\lambda=0$ to $\lambda=\lambda_c$, a pole of the T matrix moves along the negative W axis toward $W=0$. When $\lambda=\lambda_c$, the critical value of the potential strength to produce a bound state at $W=0$, this pole comes up through the cut at $W=0$, and as λ is increased beyond λ_c, the pole which now represents a true bound state moves toward $W=-\infty$ on the first sheet of the W plane. λ_c for the Yukawa potential is easily found to be $\lambda_c=1.6798084$. Figure 10 shows the movement in the $\sqrt{W}$ plane of the stationary zero of the denominator of our rational approximation as the potential strength is varied. The position of the pole for $\lambda\geq\lambda_c$ corresponds to the energy of the bound state. The numerical value of the bound-state energy obtained from this approximation agrees with other determinations to about four decimal places.

To summarize the results of this section, we have seen that this method works very well as a practical computational tool. With it we are able to calculate scattering phase shifts for a large range of momenta and potential strengths very easily and quite accurately. The method is also useful in finding the positions of bound states and can describe the behavior of the amplitude on an unphysical sheet. The accuracy of the continued amplitude depends to a large extent on the precision of the input points and also, but not so critically, on their location; generally, two decimal places of accuracy are lost in the continuation. The method is fast, simple, and accurate. Another of its virtues, still to be demonstrated, is that it can be used in a straightforward manner to calculate two-channel and three-body scattering amplitudes.

IV. TWO-CHANNEL SCATTERING

In this section, the methods of numerical analytic continuation are applied to a two-channel problem.

It is shown that the approach used for the single-channel case may be applied to this problem with only minor modifications. The new feature of the two-channel calculation is the existence of more than one scattering threshold. The solution of this problem by our methods demonstrates that the continuation approach is able to include the effects of this higher threshold. The first section is a brief discussion of the formalism. The second section is devoted to describing the modifications of the continuation method to include the higher thresholds, and the third section is a presentation of the results.

A. Two-Channel Formalism

Consider the specific two-channel problem of the scattering of a projectile of mass m and momentum p from a target that can exist in two states of energy E_1 and E_2. The wave function for such a process is the product of the projectile and the target wave function,

$$\Psi=\psi_1^T\psi_1^P+\psi_2^T\psi_2^P, \tag{4.1}$$

where ψ_i^T, ψ_i^P are the target and projectile wave functions in the channel i. Similarly, the Hamiltonian is the sum of the target and the projectile Hamiltonians,

$$\begin{aligned} H&=H_0^T+H_0^P+V,\\ H_0&\equiv H_0^T+H_0^P, \end{aligned} \tag{4.2}$$

and the target wave functions satisfy

$$H_0^T\psi_i^T=E_i\psi_i^T. \tag{4.3}$$

The Schrödinger equation for the wave function Ψ is

$$(E-H)\Psi=0, \tag{4.4}$$

and to obtain the analogous equation for ψ_i^P, we take the matrix element of (4.4) with the state ψ_i^T, which yields

$$(E-E_i-H_0^P)\psi_i^P=\sum_{j=1}^{2} V_{ij}\psi_j^P, \tag{4.5}$$

where $V_{ij}=(\psi_i^T,V\psi_j^T)$.

Since the discussion of the scattering operator for the single-channel case was really quite general, we may apply the same arguments here to obtain the equation for the two-channel T operator

$$T(W)=V+V(W-H)^{-1}V. \tag{4.6}$$

The physical T matrix is obtained as the limit as $W\to E+i\epsilon$ of the matrix element of $T(W)$ between the asymptotic states Φ satisfying

$$(E-H_0)\Phi=0. \tag{4.7}$$

As in Eq. (4.1), Φ is the product of the target and projectile wave functions,

$$\Phi=\varphi_1^P\psi_1^T+\varphi_2^P\psi_2^T,$$

and φ_i^P satisfies

$$(E-E_i-H_0^P)\varphi_i^P=0 \quad \text{or} \quad (p_i^2-H_0^P)\varphi_i^P=0,$$

where $p_i^2=E-E_i$ is the momentum of the projectile in the ith channel. The T matrix element for the transition $i\leftarrow j$ is then

$$T_{ij}(p_i,p_j,E)=\lim_{W\to E+i\epsilon}(\varphi_i^P\psi_i^T,T(W)\varphi_j^P\psi_j^T).$$

The momenta in the two channels are related by

$$p_2=(p_1^2+E_1-E_2)^{1/2},$$

and for a channel that is closed at a given energy and momentum, i.e., $p_2^2=p_1^2+E_1-E_2<0$, the asymptotic wave function $\varphi_2^P(p_2)$ is zero.

In the study of single-channel scattering, we found the unitarity condition $\mathrm{Im}[T_l(p,E)]^{-1}=p$ to be a useful check on the numerical calculations. In the same way, two-channel unitarity provides a convenient means for verifying the results of this calculation. Considering T as a matrix, the statements of two-channel unitarity are (for potentials such that $V_{12}=V_{21}$) for the partial-wave T matrix element

$$\mathrm{Im}[(T_{ij}^l)^{-1}]=\begin{bmatrix} p_0 & 0\\ 0 & p_2\end{bmatrix}. \tag{4.8}$$

Equation (4.8), when written out in terms of $T_{ij}(E)$, actually provides three conditions on the physical T matrix elements:

$$\mathrm{Im}[(T^{-1})_{11}]=\mathrm{Im}[T_{22}/(T_{11}T_{22}-T_{12}T_{21})]=p_1,$$
$$\mathrm{Im}[(T^{-1})_{22}]=\mathrm{Im}[T_{11}/(T_{11}T_{22}-T_{12}T_{21})]=p_2,$$

and

$$\mathrm{Im}[(T^{-1})_{12}]=\mathrm{Im}[T_{12}/(T_{11}T_{22}-T_{12}T_{21})]=0.$$

Since $V_{12}=V_{21}$, we also have the condition $T_{12}^l=T_{21}^l$. These statements of two-channel unitarity provide a convenient check on the numerical calculations.

B. Continuation Method in the Two-Channel Case

As in the single-channel case, we use the form

$$T(W)=V+V[W-H]^{-1}V \tag{4.9}$$

to obtain the analytic properties of T as a function of W. Knowing the spectrum of the operator H, we can

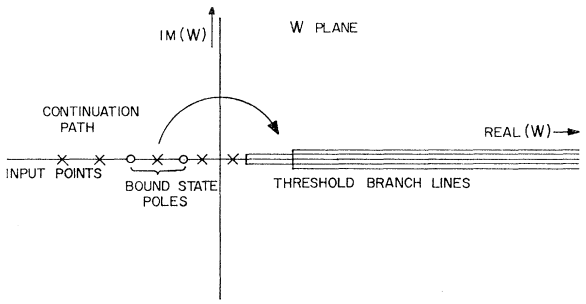

FIG. 11. Analytic structure of the two-channel scattering amplitude in the complex-energy plane.

conclude that $T(W)$ may have simple poles for real values of $W<E_1$ corresponding to bound states of H, a line of discontinuities starting at $W=E_1$ corresponding to the scattering threshold in the first channel, and a line of discontinuities at $W=E_2$ corresponding to the scattering states in the second channel. $T(W)$ is analytic everywhere else on the first sheet of the W plane, as shown in Fig. 11.

The method consists of the same two steps outlined before. First, $T_{ij}(W)$ is calculated for several values of $W<E_1$ (denoted by x's in Fig. 11). Then these numerical results are analytically continued to the physical energy, using the rational-fraction approximation, to obtain the scattering amplitudes. The inputs may be calculated using the variational principle previously discussed or by straightforward mesh-point integration of the

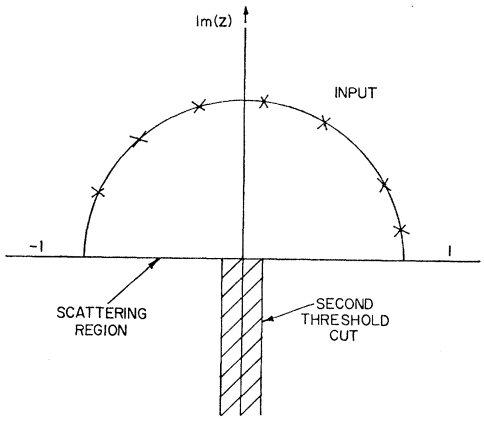

FIG. 12. Location of scattering cut and input points for the two-channel scattering amplitude in the $Z=[(-W+E_1)^{1/2}+i(E_2-E_1)^{1/2}]/[(-W+E_1)^{1/2}-i(E_2-E_1)^{1/2}]$ plane.

integral equation for $T(W)$

$$T(W)=V+V[W-H_0]^{-1}T(W), \qquad (4.10)$$

since, for $W<E_1$, Eq. (4.10) is a nonsingular equation. For our calculations, the variational principle worked quite well and was the only method used.

The new aspect of the two-channel problem is that there are two scattering thresholds rather than just one, as in the single-channel case. Since these are just two-particle scattering thresholds, $T(W)$ is analytic in the variable $(W-E_i)^{1/2}$ near the ith threshold. Representing T as the ratio of polynomials in the variable $y=(-W+E_1)^{1/2}$, we take into account the first threshold, but the second threshold then occurs at $y=\pm i(E_2-E_1)^{1/2}$. The transformation

$$Z=[y+i(E_2-E_1)^{1/2}]/[y-i(E_2-E_1)^{1/2}]$$

transforms these branch points to $Z=0$ and $Z=\infty$; in the Z plane, the situation is shown in Fig. 12, where we now draw the branch line from $Z=0$ to $Z=\infty$. In the variable $Z'=\sqrt{Z}$, the second threshold is taken into account, and an everywhere analytic function of $(W-E_1)^{1/2}$ and $(W-E_2)^{1/2}$ is an everywhere analytic function of Z'. This process, known as uniformization,[13] may be used in a similar manner to include more thresholds, although the transformations and the mapping of the complex plane become more complicated with each additional threshold. To include the effects of the two scattering thresholds, $T(W)$ is represented as a ratio of polynomials in the variable

$$Z'=\left[\frac{(-W+E_1)^{1/2}+i(E_2-E_1)^{1/2}}{(-W+E_2)^{1/2}-i(E_2-E_1)^{1/2}}\right]^{1/2}.$$

After incorporating this minor change into the method, the continuation technique, as described in the previous sections, may be used directly to obtain two-channel scattering amplitudes.

TABLE IV. Successive approximations to $(\tan\delta)/p_1$ and elastic unitarity $[\mathrm{Im}[(T^{-1})_{11}/p_1]=1]$ for the potentials $V_{11}=-2e^{-r}/r$, $V_{22}=e^{-r}/r$, $V_{12}=V_{21}=-0.5e^{-r}/r$ for the momentum in channel 1; $p_1=0.1$ and $E_2=0.04$ (channel 2 closed).

	Second threshold not included		Second threshold included	
N	$(\tan\delta)/p_1$	Unitarity	$(\tan\delta)/p_1$	Unitarity
1	6.8006	1.0026	6.279679	0.684
2	6.77634	1.0013	6.7924596	0.9767
3	6.780024	0.9997	6.7814632	1.0002
4	6.7801627	0.9995	6.7814660	1.00005
5	6.781097	0.999998	6.7808974	1.00002
6	6.7811055	0.999998	6.7809548	1.000008
7	6.7811085	0.999997	6.7809558	1.000008

C. Two-Channel Results

The numerical examples chosen to describe this method are calculations of S-wave scattering in the Yukawa potentials

$$V_{11}=\lambda_1 e^{-r}/r, \quad V_{22}=\lambda_2 e^{-r}/r, \quad V_{12}=V_{21}=\lambda_{12}(e^{-r}/r).$$

The point or continued-fraction method was used to calculate successive approximations to the scattering amplitudes for the sequence $N=1, 2, 3, \cdots$, where $2N+1$ is the number of input points at each stage, and N also equals the order of the polynomials in the numerator and denominator of the rational fraction. For this numerical example, $E_1=0$ and E_2 was varied. The input points were distributed along the negative W axis in accordance with the transformation (3.13), with a arbitrarily chosen as -0.4. As before, the accuracy of the input decreased with increasing momentum.

In Table IV, we show the results of this type of calculation for $E_2=0.04$, $\lambda_1=-2$, $\lambda_2=+1$, $\lambda_{12}=-0.5$ for the momentum $p=0.1$. At this value of the momentum, the second channel is closed, and there is only one amplitude, $T_1(p,E)$, which may be represented, as in

[13] R. G. Newton, *Scattering Theory of Waves and Particles* (McGraw-Hill Book Co., Inc., New York, 1966).

the single-channel case, as

$$T_{11}(p,E)=e^{i\delta}(\sin\delta)/p.$$

The unitarity condition in this case reduces to

$$\mathrm{Im}[T^{-1}(p,E)]_{11}=p.$$

The first two columns of Table IV show $(\tan\delta)/p$ and $\mathrm{Im}[T^{-1}(p,E)]_{11}/p$, where only the first threshold was included in the continuation. The second two columns of this table give the same quantities as obtained from the rational approximation in which both thresholds were included. The results for the two methods agree to about three parts in 10^5, and similar results were obtained in all cases for momenta such that the second channel is closed. Thus we can conclude that below the "inelastic" threshold, this approximation yields good results even if the second threshold is not included in the representation. We believe that the reason that the second representation is not considerably better than the first is that the approximation not including the second threshold is in the variable $W^{1/2}$, while the variable is essentially $W^{1/4}$ for the approximation which includes the second threshold. The first representation has twice as many whole powers of W for a given order N than the second type, and is better able to approximate the gross behavior of $T(W)$ for that reason.

Above the inelastic threshold, however, the improvement obtained by including the second threshold is marked. In Table V, we compare the three unitarity conditions for the T matrix elements evaluated by these two methods for the parameters $\lambda_1=-2$, $\lambda_2=1$, $\lambda_{12}=-0.5$, $p_1=0.3$, and $p_2^2=0.05$. The first three columns are the results of the continuation ignoring the second threshold, and the last three columns are the results obtained when the second threshold is included. The results for the T matrix displayed roughly the same convergence in both cases, but differed in value by about 1%.

As a final example of the results of this two-channel calculation, we show in Table VI the successive approximations to the real parts of $T_{11}(p_1)$, $T_{22}(p_2)$, and $T_{12}(p_1,p_2)$, and the unitarity conditions for the parameters $\lambda_1=-2$, $\lambda_2=1$, $\lambda_{12}=3$. Again the convergence is very good. The method yielded the same accuracy for almost all the parameters that were tried. In the special case $|\lambda_1|\sim|\lambda_2|\sim|\lambda_{12}|$ and p above the second threshold, it happens that $T_{11}\sim T_{12}\sim T_{22}$, and the determinant of the T matrix is nearly zero. For this special case, although the results of the calculation were nicely convergent, the calculated unitarity conditions were very poor.

To summarize, we have shown that the continuation method, with only minor modifications, is able to handle the new feature of the two-channel problem. The effects of the inelastic threshold are included in the representation by uniformization of the amplitude, and, although the errors incurred by the neglect of the second threshold are not large, inclusion of both thresholds increases the accuracy of the calculation, especially above the second threshold. It is clear from these examples that the continuation method is a practical approach to the numerical solution of two-channel-scattering problems.

V. CONCLUSIONS

The rational-fraction approximation discussed in Sec. II is a useful technique for numerical analytic continuation. This type of approach should be useful in a broader range of problems than those discussed here.

TABLE V. Successive approximations to the three unitarity conditions for the two-channel T matrix for the potentials $V_{11}=-2e^{-r}/r$, $V_{22}=e^{-r}/r$, $V_{12}=V_{21}=-0.5\,e^{-r}/r$ for the momenta $p_1=0.3$, $p_2^2=0.05$, and $E_2=0.04$.

	Second threshold not included			Second threshold included		
N	$\mathrm{Im}[(T^{-1})_{11}/p_1]$	$\mathrm{Im}[(T^{-1})_{22}/p_2]$	$\mathrm{Im}[(T^{-1})_{12}]$	$\mathrm{Im}[(T^{-1})_{11}/p_1]$	$\mathrm{Im}[(T^{-1})_{22}/p_2]$	$\mathrm{Im}[(T^{-1})_{12}]$
1	0.998	0.0407	2×10^{-3}	1.166	0.036	4×10^{-3}
2	0.993	0.204	8×10^{-3}	1.015	0.276	3×10^{-2}
3	0.9994	0.697	5×10^{-3}	1.0091	1.039	8×10^{-4}
4	0.995	0.961	3×10^{-3}	0.9964	1.0084	4×10^{-4}
5	1.001	1.128	3×10^{-3}	1.00007	1.0041	2×10^{-4}
6	0.99998	1.01	2×10^{-4}	0.9999916	0.99994	5×10^{-6}
7	0.999994	1.01	2×10^{-4}	0.9999913	1.0000004	5×10^{-6}

TABLE VI. Successive approximations to $\mathrm{Re}[T_{11}]$, $\mathrm{Re}[T_{22}]$, $\mathrm{Re}[T_{33}]$ and two-channel unitarity for the potentials $V_{11}=-2e^{-r}/r$, $V_{22}=e^{-r}/r$, $V_{12}=V_{21}=3e^{-r}/r$; $p=0.4$, $E_2=0.04$. Both thresholds have been included in the continuation.

N	$\mathrm{Re}[T_{11}]$	$\mathrm{Re}[T_{22}]$	$\mathrm{Re}[T_{12}]$	$\mathrm{Im}[T_{11}^{-1}/p_1]$	$\mathrm{Im}[T_{22}^{-1}/p_1]$	$\mathrm{Im}[T_{12}^{-1}]$
1	−0.165	0.932	−0.62	0.944	0.07	2×10^{-2}
2	1.02	0.851	0.115	0.918	0.34	9×10^{-2}
3	1.06	0.855	0.148	1.01	0.96	4×10^{-3}
4	1.098276	0.851	0.162	1.003	0.9996	5×10^{-4}
5	1.098621	0.84916	0.15996	0.9991	0.9976	6×10^{-4}
6	1.098346	0.84927	0.160568	1.00001	1.00003	6×10^{-6}
7	1.098346	0.84927	0.160568	1.000009	1.000003	2×10^{-6}

Although some rules governing the convergence of these expansions were described in terms of simple examples, we believe that further investigation in this field must be based on a rigorous mathematical foundation.

The method of analytic continuation has been applied here to the calculation of two-body and two-channel amplitudes, and our results for some three-body processes will be given in a subsequent communication. From these examples it is clear that the continuation method is a useful computational tool for the study of a wide range of physical problems. One limitation of the method is the lack of a convergence theorem for the rational-fraction method of analytic continuation. It is therefore important that one have an independent check on the continued value of the function (the unitarity condition in this case). We see no difficulty, in principle, of extending these results to multichannel or even multiparticle scattering. The method is easy to apply, can yield accurate results, and represents a simple approach to nonrelativistic-scattering computations.

ACKNOWLEDGMENTS

The author is indebted to Professor C. Schwartz, who suggested this problem, for his continued guidance and encouragement, and would like to thank Professor K. Miller, Dr. R. Haymaker, and Dr. J. Wright for several discussions. Much of the work reported here was done while the author was a National Aeronautics and Space Administration Trainee at the University of California, Berkeley.

APPENDIX

Consider the continued fraction (2.9)

$$C_N(x)=\frac{f(x_1)}{1+}\,\frac{a_1(x-x_1)}{1+}\,\frac{a_2(x-x_2)}{1+}\cdots\frac{a_N(x-x_N)}{1}.$$

For our approximation we demand that $C_N(x_{l+1})=f(x_{l+1})$, or

$$C_N(x_{l+1})=f(x_{l+1})=\frac{f(x_1)}{1+}\,\frac{a_1(x_{l+1}-x_1)}{1+}\cdots\frac{a_l(x_{l+1}-x_l)}{1}. \quad \text{(A1)}$$

Equation (A1) may be written as

$$f(x_1)/(1+Z_1)=f(x_{l+1}), \quad \text{(A2)}$$

where

$$Z_1=\frac{a_1(x_{l+1}-x_1)}{1+}\,\frac{a_2(x_{l+1}-x_2)}{1+}\cdots\frac{a_l(x_{l+1}-x_l)}{1}.$$

Solving (A2) for Z_1 yields

$$Z_1=-\{1-[f(x_1)/f(x_{l+1})]\}. \quad \text{(A3)}$$

But

$$Z_1=\frac{a_1(x_{l+1}-x_1)}{1+Z_2},$$

where

$$Z_2=\frac{a_2(x_{l+1}-x_2)}{1+}\cdots\frac{a_l(x_{l+1}-x_l)}{1}.$$

Writing (A3) as

$$\frac{a_1(x_{l+1}-x_1)}{1+Z_2}=-\left[1-\frac{f(x_1)}{f(x_{l+1})}\right]$$

and solving for Z_2 yields

$$Z_2=-1-\frac{a_1(x_{l+1}-x_1)}{1-[f(x_1)/f(x_{l+1})]}. \quad \text{(A4)}$$

Continuing in this way, we set

$$Z_2=\frac{a_2(x_{l+1}-x_2)}{1+Z_3}$$

in (A4) to obtain

$$Z_3=\frac{a_3(x_{l+1}-x_3)}{1+Z_4}=-\left\{1+\frac{a_2(x_{l+1}-x_2)}{1+}\,\frac{a_1(x_{l+1}-x_1)}{1-[f(x_1)/f(x_{l+1})]}\right\}.$$

Repeating this process yields the result

$$a_l(x_{l+1}-x_l)=-\left\{1+\frac{a_{l-1}(x_{l+1}-x_{l-1})}{1+}+\frac{a_{l-2}(x_{l+1}-x_{l-2})}{1+}\cdots\frac{a_1(x_{l+1}-x_1)}{1-[f(x_1)/f(x_{l+1})]}\right\},$$

which is Eq. (2.10).

Equation (2.10) is an explicit formula for a_l in terms of the x_i, $f(x_i)$, and a_{l-1}, a_{l-2}, $\cdots$, a_1. As the order of the approximation is increased from N to $N+1$, all the a's remain the same, while a_{N+1} as given by (2.10) is added to the expression (2.9).